60 M stomach ca. liver met.

Fig. 4. Enhanced permeability and retention (EPR) effect. (a) A S180 tumor on the skin of a mouse. The tumor shows relatively homogeneous uptake of Evans blue/albumin, but normal skin in the background contains no blue color.[5,76–79] (b) Heterogeneity of the EPR effect. Only the tumor periphery took up Evans blue/albumin. (c) Blood vessels in normal liver had no leakage of polymer resin. (d) Metastatic tumor nodule (N) in liver, approximately 200 μm in diameter, showed distinct extravasation of polymer resin in small nodules (T). (e) Computed tomography of a patient that shows selective uptake of Lipiodol in a tumor (white area) in the liver that was metastatic (met.) from gastric cancer (ca.): two tumors (arrows) are intensely stained (white) by Lipiodol. Styrene–maleic acid copolymer conjugated with neocarzinostatin/Lipiodol was infused into the hepatic artery under angiotensin II-induced hypertension (see text, and refs 79 and 89. 60 M, patient, 60 yr old male; SX i.a. AT, SMANCS given via ia route under angiotensin II induced hypertension. (e') Computed tomography of the same patient approximately 1 month later, showing a considerably reduced tumor size (arrows). Drug retention lasted for more than 1 month. (f) Relationship between radiolabeled polymers of N-(2-hydroxypropyl) methacrylamide (P-HPMA) various molecular sizes and their uptake by tumor, kidney, and liver. The EPR effect depended on time (6 h vs 5 min is shown). conc, concentration. (g) Relationship between the molecular size of drugs and tumor uptake of drug (○), urinary clearance (CL, ●), and area under the concentration versus time curve (AUC) of plasma (▲).[12,15,77]

selectivity and high antitumor potency. With Toshimitsu Konno, M.D., a surgeon, we developed one of the most effective tumor-targeting methods, arterial infusion of SMANCS dissolved in Lipiodol. Because of its high lipophilicity, despite it being a macromolecule, SMANCS could be dissolved in Lipiodol and a homogeneous solution could be obtained. We believed that SMANCS/Lipiodol would penetrate the interstitial tumor tissue directly through the tumor's vascular walls after arterial infusion given into the tumor-feeding artery. This technique was the first theranostic approach (see later), in that the uptake of Lipiodol by the tumor tissue allowed highly sensitive X-ray visualization of the tumor, preferably CT.[75,81–90]

Quantitative evaluation of uptake by the tumor of ^{14}C-labeled Lipiodol that we synthesized showed the extremely high tumor selectivity of this approach: the tumor Lipiodol concentration was 2000 times higher than that of blood at 15 min after, and more than 3000 times higher at 3 days after intra-arterial infusion.[75,81] The imaging potential with an X-ray system was thus clear.[82–85] These results were then applied to difficult-to-treat human tumors, specifically hepatoma and other abdominal and renal cancers, with or without angiotensin II-induced hypertension, which augmented drug delivery.[84,87–89] Tumors such as metastatic liver cancer and cancers of the gallbladder, pancreas, liver, and kidney responded quite well to this treatment.[89] A marked therapeutic effect and diagnostic value, even early detection, were obtained. Also, as a unique result, estimation of

the level of drug (SMANCS/Lipiodol) delivered to the tumor using CT became possible (Fig. 4e,e'). This protocol produced very few adverse effects such as bone marrow suppression or anorexia. Also, the prolonged retention of drug in the tumor meant less frequent drug administration (once in 3–4 months) was required, so that patient compliance was quite good.

As an extension of this method, bronchoarterial infusion of ISDN (Nitrol®, Eisai, Tokyo. Japan), which also enhanced tumor blood flow and drug delivery, followed by intra-arterial infusion of SMANCS/Lipiodol for advanced lung cancer gave very encouraging results.[90] Several reports provide descriptions of these results.[1,22,76,77]

Influences on and augmentation of the EPR effect

Architectural differences in tumor vasculature. The enhanced vascular permeability of solid tumors depends on two features. One is the microanatomical architecture of tumor blood vessels, which was observed by electron microscopy.[72–74,91,92] The tumor vasculature was extremely irregular, for example: the vascular network branched and stretched; endothelial cell–cell junctions had large gaps between them, with pores as large as 4 μm rather than the <10-nm pores of normal vessels[92]; the vascular diameter was larger, with a uniquely irregular shape, and frequently missing pericytes or the smooth muscular layer that surrounds blood vessels; and leakage of acrylic polymer resin occurred, similar to leakage of albumin into the

interstitial space, as seen in Figure 4(a,b).[72–74,76,77] The second feature concerns vascular mediators, as described below.

Factors that facilitate the EPR effect and artificial augmentation of the effect. *Pharmacological factors that facilitate the EPR effect.* As described earlier, we began our study of vascular permeability in the bacterial infection and activation of the kallikrein cascade, which resulted in the generation of kinin (Fig. 1).[15–22] This same mechanism was found to occur in cancer tissues.[15,16,18,32–34] We subsequently determined that NO, ONOO⁻, carbon monoxide, prostaglandins, and collagenases among others, are mediators that facilitate the EPR effect (Fig. 3a,c,d),[17,19,21,94] as summarized in Table 1. Recent reviews give good accounts on these issues.[21,76–79]

Augmentation of the EPR effect. With the above-described knowledge in hand, we continued to develop methods of augmenting the EPR effect for drug delivery to tumors. We first infused angiotensin II i.v.,[12] during the arterial infusion of SMANCS/Lipiodol, to raise the blood pressure, as discussed earlier.[70,89] This strategy takes advantage of the architectural defects of tumor vessels to make drugs more permeable. The second method used NO-releasing agents such as nitroglycerin, ISDN, and others, which are known to be quite safe.[77,90,96] Frequently, the tissue of many tumors is hypoxic compared with normal tissues, similar to infarcted heart tissue. This situation means that denitrase is involved in NO formation by reducing nitrite to NO, as Figure 3(d) shows. This process of NO generation is preferred by hypoxic tissues such as metastatic cancers and other hypoxic cancers of the prostate and pancreas. Yasuda, Jordan, and Mitchell and their colleagues also showed the use of NO-releasing agents to be beneficial in conventional cancer chemotherapy in terms of redox modulation.[98–102]
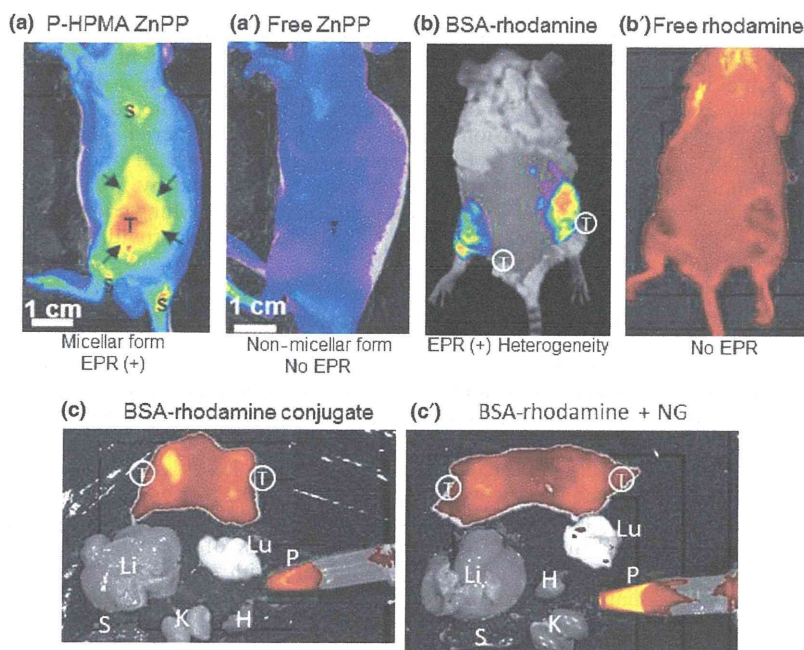
The third method uses bradykinin-potentiating agents such as inhibitors of angiotensin I-converting enzyme to inhibit kinin degradation in tumor tissue, which would result in a higher kinin level at the site of kinin generation (tumor) (Fig. 1).[19–21,34,103] All these methods enhanced the EPR effect and thereby drug delivery by two- to threefold. The limited clinical applications have indicated the potential for delivery of SMANCS/Lipiodol to tumors, as noted in descriptions of methods using elevated blood pressure[89] or ISDN,[90] which warrants further exploration.

Heterogeneity of the EPR effect. The heterogeneity of the EPR effect poses a problem in that some areas of tumor tissue resist the uptake of drugs (of nanomedicines) for both chemotherapy and tumor imaging (see below), and drugs have great difficulty reaching the tumor interstitium.[76–79] However, we demonstrated that augmentation of the EPR effect led to result in a more uniform and enhanced drug delivery.[76–79,89] Large necrotic areas of tumor (as seen in Fig. 4b *vs* 4a) did not show uptake of Evans blue/albumin, whereas the EPR effect was more prominent at the tumor periphery, where tumor growth is rapid.[76–79,89] Angiography revealed that pancreatic and prostate cancers are hypovascular (so, less uptake of the contrast agent occurs). However, even in these hypovascular tumors, angiotensin II-induced hypertension seemed to improve drug delivery to tumors (Fig. 4e,e').[70,77,88]

Enhanced permeability and retention (EPR) effect in tumor imaging

We first demonstrated the use of the EPR effect in tumor imaging by injecting Evans blue dye i.v., so that the blue tumor could be visualized (Fig. 4a).[5,15,21,22,76–79] To make tumor detection more sensitive, we recently developed fluorescent-labeled macromolecules, named fluorescent nanoprobes.[79,104]

Figure 5(a) compares detection using low-molecular-weight free ZnPP and macromolecular HPMA polymer conjugated with ZnPP. The free low-molecular-weight fluorophore (ZnPP, molecular size 626.0) does not show tumor-selective uptake (Fig. 5a'), whereas the polymer-conjugated ZnPP showed marked tumor-selective uptake and remained in the tumor even after 48 h (Fig. 5a).[104] Another example involves free rhodamine B (molecular size 479.0) versus rhodamine isothiocyanate-conjugated albumin (67 kDa). Here again, the EPR effect-based tumor uptake was demonstrated and was unique for macromolecular probes but not for free rhodamine B or ZnPP (Fig. 5b *vs* 5b').[79] These tumor images were obtained by using the *in vivo* fluorescence detection system IVIS XR (Caliper Life Sciences, Hopkinton, MA, USA) with intact animals. This finding suggests that fluorescent endoscopy for detecting human tumors should be possible. Treatment with the NO-releasing

(a) P-HPMA ZnPP **(a')** Free ZnPP **(b)** BSA-rhodamine **(b')** Free rhodamine

Micellar form EPR (+) Non-micellar form No EPR EPR (+) Heterogeneity No EPR

(c) BSA-rhodamine conjugate **(c')** BSA-rhodamine + NG

Fig. 5. (a,b) Staining of tumors (T) with fluorescent nanoprobes and free low-molecular-weight probes. (a) Polymer N-(2-hydroxypropyl) methacrylamide (P-HPMA)-conjugated zinc protoporphyrin ZnPP (micelles). (b) Rhodamine-conjugated BSA. These drugs were given i.v. and show clear tumor-selective fluorescence. The low-molecular-weight fluorescent counterparts, free ZnPP and free rhodamine B (images (a') and (b'), respectively), manifested no tumor-selective fluorescent staining. EPR; enhanced permeability and retention effect. (c) Fluorescence after surgical organ removal, only tumor (T) and blood plasma (P) showed fluorescent staining. (c') is same as (c) except that this mouse was treated with nitroglycerin (NG). Results here show a more uniform tumor delivery (T) and higher plasma level of the nanoprobes than seen in (c). H, heart; K, kidney; Li, liver; Lu, lung; S, spleen.

Steps	Barriers to be overcome	Comments
1	**Vascular wall**/Circulating blood **EPR effect**/Extravasation into tumor tissue Tumor tissue/interstitial space	Polymeric drugs/nanomedicines Vascular wall openings Enhancement of the EPR effect by NO and angiotensin-converting enzyme inhibitor
2	Dissemination to tumor cells	Stromal matrix/fibrin gel/fibroblast protease/plasmin/plasminogen activator
3	Cell membrane/**internalization**	**Endocytic uptake** **Styrene-co-maleic acid (SMA) micelle disintegration**
4	**Drug release**/free active drug pH/protease-labile linker Interact with target molecules	No reverse exocytosis Hydrazone/maleic acid help drug release
5	*In vivo* antitumor effect: 100% survival/cure	React with target molecules High antitumor efficacy *in vivo*
6	**Regulatory steps/safety issue**	Phase I, II, III trials
7	**Cost/benefit**	More universal tumor targets [Evaluation by Natl. Inst. Health Clin. Excellence, UK]

Fig. 6. Barriers to targeting of drugs to tumors before the target molecules in tumor cells are reached, from the vascular level to the molecular target at the subcellular level. EPR, enhanced permeability and retention.
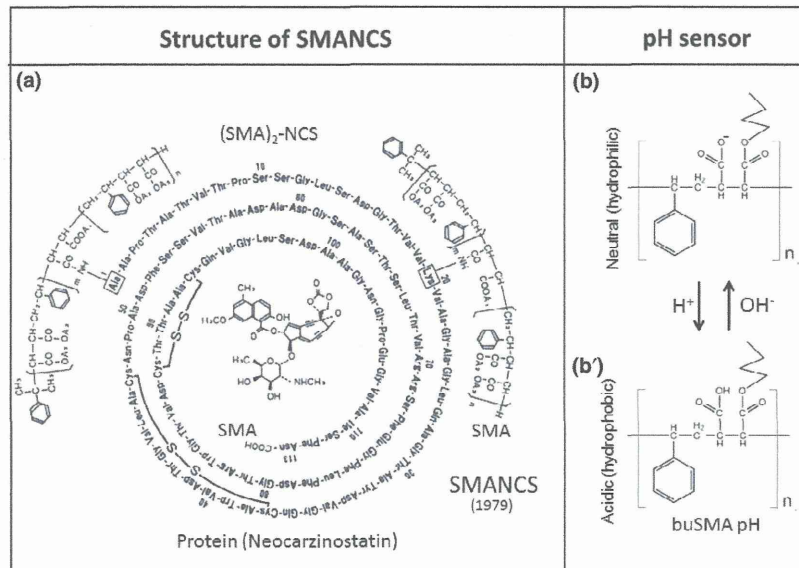

Fig. 7. Chemical structure of styrene–maleic acid copolymer conjugated-neocarzinostatin (SMANCS), and the styrene–maleic acid copolymer (SMA) residue as a pH sensor and lipophilicity enhancer. (a) Chemical structure of SMANCS, which consists of a protein portion of neocarzinostatin (NCS) and two chains of SMA copolymers linked at the N-terminal alanine and at lysine 20. (b,b′) Close-up views of the SMA unit with styrene and maleyl residues, in which the maleyl carboxyl group has the role of a pH sensor. In acidic pH (b′), the R-COOH of maleyl residues becomes to COOH, which possesses higher lipophilicity than does the COO⁻ form. SMANCS would thus have greater cell-binding affinity, a more than 10 to 100-fold higher cellular uptake in weakly acidic pH, with cytotoxicity increasing in parallel. (b) At neutral or higher pH of normal tissues, deprotonation occurs, with formation of the negatively charged R-COO⁻ and more hydrophilicity of SMANCS.[109–112] Cell interaction is thus impeded and internalization into cells is lower. buSMA indicates the *n*-butylated ester form of maleyl residues in SMA, in which approximately 37 mol% maleyl residues of SMA are replaced for proton and the remaining carboxyl residues are free.

agent nitroglycerin in this model produced a more uniform uptake in the tumor and elevated and prolonged plasma drug concentration, which favor a greater EPR effect (Fig. 5c *vs* 5c′).

A unique property of ZnPP is that it not only emits fluorescence during endoscopic imaging with xenon light irradiation, it also generates singlet oxygen ($^1O_2$), which has cytocidal effects on tumor cells, the result being significant tumor regression and cure in an *in vivo* model.[104] This theranostic approach was confirmed with ZnPP–SMA micelles in autochthonous breast cancer in Sprague–Dawley rats *in vivo*.[105]

The term theranostic was coined by Funkhouser in 2002[106] and is becoming quite popular. A recent comprehensive review of this topic can be found in ref. 107.

Drug uptake by tumor cells and drug release from nanomedicines

Interactions with the cell surface: Influence of charge and hydrophobicity. The most desirable anticancer agents must ultimately possess properties to overcome various barriers, as

given in Figure 6.[79] The first, most crucial barrier is the vascular wall, and the EPR effect plays a key role here. To take advantage of the EPR effect, drugs must have macromolecular characteristics (or nanomedicines), which permit selective extravasation into tumor tissues but not normal tissues (Figs 4,5).

Among other critical steps, cellular internalization of drugs is indispensable and can be a great barrier to therapeutic effectiveness (Fig. 6). A contradictory issue exists in the interaction between nanoparticles and cell surfaces of normal as well as tumor cells. Requisites for the EPR effect include a sustained high concentration of nanomedicines in plasma during circulation that requires less interaction of nanomedicines with surfaces of cells such as vascular endothelial cells, and escape of nanomedicines from clearance by phagocytic cells. In this respect, the "stealth" characteristic of PEGylated and HPMA-polymer conjugates is now known as a favorable feature. Hatakeyama et al. reported, however, that such stealth nanoparticles are poorly taken up by cancer cells.[108] In our laboratory, we compared HPMA-, PEG-, and SMA-conjugated micelles, and found that among these, SMA conjugates had the highest cellular uptake, whereas both PEG- and HPMA-polymer conjugates had much less efficient cellular uptake.[109]

In our earlier studies of SMANCS, we showed that conjugation of SMA conferred far greater cellular uptake, which corresponded to cytotoxicity.[11,110,111] That is, more efficient cellular uptake (50 to 100-fold) occurred with the hydrophobic SMA-polymer conjugate (SMANCS) than with the parental NCS, and more potent cytotoxicity (20 to 100-fold) was observed in a weakly acidic environment, as in tumors, than in the neutral pH of normal tissues. In the weakly acidic setting, the protonated (COOH) form of the maleyl residue in SMA has stronger hydrophobicity and a higher affinity for cell membranes than does the ionized COO^- form of SMA (see Fig. 7b vs 7b').[11,110,111] Also, many cell surfaces are negatively charged, so that interaction with negatively charged nanoparticles is repelled, which results in less cellular uptake. Maleyl carboxyl residues would therefore provide a pH-sensing property in the tumor environment.

These results show that hydrophobicity and charge are important for the cell-binding property. However, this hydrophobic feature should be carefully controlled, or hemolysis or cell lysis may be induced.[112] This hydrophobic property of cell lysis and strong anionic nature would also cause rapid uptake by the liver or spleen. These effects may be another drawback, but they can be controlled by proper modification of the carboxyl group (Tsukigawa K and Maeda H, unpublished data).

Drug release from drug complexes or carriers. Release of drugs from nanoparticles is another critical step for tumor-selective drug delivery. We found that HPMA–ZnPP and SMA–ZnPP micelles, for example, disintegrated during endocytosis, not during circulation, and that disintegration in the cell made the drug more accessible to the target molecules.[109] A similar phenomenon of disruption of micelles was seen after treatment with lecithin or detergent.[109] Many researchers conjugated active ingredients to the polymers using specific protease-cleavable peptides with preferred amino acid sequences, or ester or other chemical bonds.[113] For example, SMA was conjugated to NCS by amide bonds in SMANCS, and the maleyl amide underwent spontaneous hydrolysis in acidic pH. In addition, the hydrazone linker bond between the polymer and ZnPP spontaneously released ZnPP in the weakly acidic pH of tumor tissues (Nakamura H, Subr V, Ulbrich K, Maeda H, unpublished data, 2013). We also found disruption of an SMA–cisplatin complex on endocytosis or incubation at weakly acidic pH was 6–7-fold faster than that at neutral pH (Saisyo A, Maeda H, and Nakamura H, unpublished data, 2013). Also, micelles or liposomes should be stable during

circulation but release the drug as it arrives at the tumor site is needed. Many improved ways to control the release of drugs from conjugates or complexes as based on the condition of the tumor environment are thus anticipated.

Conclusion

The vascular permeability of infected, inflamed, and tumor tissues results from multiple factors such as vascular mediators listed in Table 1, and architectural defects in tumor vessels, as described earlier. This phenomenon occurs especially with macromolecules and nanoparticles, but tumor tissue manifests great differences in this phenomenon, in that it tends to retain macromolecules in the tissue interstitium for far longer than does normal inflamed tissue. We named this phenomenon the EPR effect of macromolecules in cancer. SMANCS (Fig. 7a) was the first polymer conjugate that we developed that possesses the EPR effect.[69,77,79,84,89]

Different mechanisms participate in the generation of ROS and RNS in infected, inflamed, and cancer tissues. These mechanisms include $ONOO^-$, a product of O_2^- and NO, which is one of the most potent oxidizing, nitrating, and DNA/RNA-cleaving molecules that is involved in mutagenesis, drug resistance, carcinogenesis, vascular permeability, and tumor metastasis (Fig. 3).

We previously demonstrated the EPR effect using Evans blue (Fig. 4a,b), but it can also be visualized by using fluorescent probe-labeled macromolecules for tumor imaging in vivo (Fig. 5). However, the EPR effect as seen with Evans blue albumin staining is heterogeneous (Fig. 4b), which may impede uniform macromolecular drug delivery. This poor drug delivery to an area of a tumor with an apparently low EPR effect may be augmented by raising systemic blood pressure using slow infusion of angiotensin II or prodrugs of vascular mediators such as nitroglycerin.

To achieve efficient nanomedicine drug delivery to tumors on the basis of the EPR effect, a number of barriers, such as molecular size, surface charge, hydrophobicity, and drug release, must be overcome (Fig. 6). Differences between the environments of tumor tissues and normal tissues can be exploited to achieve greater tumor-selective drug release at the cellular level; examples include the weakly acidic pH of tumor tissues by using the hydrazone bond, and by using tumor-secreted proteases such as cathepsin or collagenases to cleave linker peptides. All these effects are more important in vivo than in cell-free systems or at the molecular level.

We are now working on endoscopic detection of tumors at a very early stage by using light irradiation of tumors to generate ROS, that is, phonon-generated singlet oxygen, as the active principle. We have developed fluorescent nanoprobes such as polymer-bound ZnPP that show tumor-selective accumulation and that, together with tumor-selective generation of ROS, will kill tumor cells in situ.[104] Such a theranostic approach will provide a highly tumor-selective therapeutic method to achieve the least invasive and most patient-friendly cancer treatment.

Acknowledgments

Disclosure Statement

The author has no conflicts of interest.

Abbreviations

AUC	area under the concentration versus time curve
CT	computed tomography
EPR	enhanced permeability and retention
HPMA	N-(2-hydroxypropyl) methacrylamide
ISDN	isosorbide dinitrate
NCS	neocarzinostatin
NO	nitric oxide
NOS	nitric oxide synthase
Nox	NADPH oxidase
O_2^-	superoxide anion radical
ONOO$^-$	peroxynitrite
P-HPMA	polymer of N-(2-hydroxypropyl) methacrylamide
Pyran copolymer	copolymer of divinylether-maleic acid
RNS	reactive nitrogen species
ROS	reactive oxygen species
SMA	styrene–maleic acid copolymer
SMANCS	styrene–maleic acid copolymer conjugated with neocarzinostatin
SOD	superoxide dismutase
XO	xanthine oxidase
ZnPP	zinc protoporphyrin

References

1 Maeda H, Konno T. Metamorphosis of neocarzinostatin to SMANCS: chemistry, pharmacology and clinical effect of the first prototype anticancer polymer therapeutic. In: Maeda H, Edo K, Ishida N, eds. *Neocarzinostatin: The Past, Present, and Future of an Anticancer Drug*. Tokyo: Springer-Verlag, 1997; 227–67.

2 Maeda H, Takeshita J, Kanamaru R. A lipophilic derivative of neocarzinostatin. A polymer conjugation of an antitumor protein antibiotic. *Int J Pept Protein Res* 1979; **14**: 81–7.

3 Maeda H, Ueda M, Morinaga T, Matsumoto T. Conjugation of poly (styrene-co-maleic acid) derivatives to the antitumor protein neocarzinostatin: pronounced improvements in pharmacological properties. *J Med Chem* 1985; **28**: 455–61.

4 Maeda H, Takeshita J, Kanamaru R, Sato H, Khatoh J, Sato H. Antimetastatic and antitumor activity of a derivative of neocarzinostatin: an organic solvent- and water-soluble polymer-conjugated protein. *Gann* 1979; **70**: 601–6.

5 Matsumura Y, Maeda H. A new concept for macromolecular therapeutics in cancer chemotherapy: mechanism of tumoritropic accumulation of proteins and the antitumor agent smancs. *Cancer Res* 1986; **46**: 6387–92.

6 Maeda H, Matsumura Y. Tumoritropic and lymphotropic principles of macromolecular drugs. *Crit Rev Ther Drug Carrier Syst* 1989; **6**: 193–210.

7 Takeshita J, Maeda H, Kanamaru R. In vitro mode of action, pharmacokinetics, and organ specificity of poly(maleic acid-styrene)-conjugated neocarzinostatin, SMANCS. *Gann* 1982; **73**: 278–84.

8 Maeda H, Matsumoto T, Konno T, Iwai K, Ueda M. Tailor-making of protein drugs by polymer conjugation for tumor targeting: a brief review on Smancs. *J Protein Chem* 1984; **3**: 181–93.

9 Kobayashi A, Oda T, Maeda H. Protein binding of macromolecular anticancer agent SMANCS: characterization of poly(styrene-co-maleic acid) derivatives as an albumin binding ligand. *J Bioact Compat Polym* 1988; **3**: 319–33.

10 Oka K, Miyamoto Y, Matsumura Y *et al.* Enhanced intestinal absorption of a hydrophobic polymer-conjugated protein drug, smancs, in an oily formulation. *Pharmaceut Res* 1990; **7**: 852–55.

11 Miyamoto Y, Oda T, Maeda H. Comparison of the cytotoxic effects of the high- and low-molecular-weight anticancer agents on multidrug-resistant Chinese hamster ovary cells in vitro. *Cancer Res* 1990; **50**: 1571–75.

12 Noguchi Y, Wu J, Duncan R *et al.* Early phase tumor accumulation of macromolecules: a great difference in clearance rate between tumor and normal tissues. *Jpn J Cancer Res* 1998; **89**: 307–14.

13 Seymour LW, Miyamoto Y, Maeda H *et al.* Influence of molecular weight on passive tumour accumulation of a soluble macromolecular drug carrier. *Eur J Cancer* 1995; **31**: 766–70.

14 Maeda H, Seymour LW, Miyamoto Y. Conjugates of anticancer agents and polymers: advantages of macromolecular therapeutics in vivo. *Bioconj Chem* 1992; **3**: 351–62.

15 Maeda H, Wu J, Sawa T, Matsumura Y, Hori K. Tumor vascular permeability and the EPR effect in macromolecular therapeutics. *J Control Release* 2000; **65**: 271–84.

16 Maeda H, Matsumura Y, Kato H. Purification and identification of [hydroxyprolyl³]bradykinin in ascitic fluid from a patient with gastric cancer. *J Biol Chem* 1988; **263**: 16051–54.

17 Maeda H, Noguchi Y, Sato K, Akaike T. Enhanced vascular permeability in solid tumor is mediated by nitric oxide and inhibited by both new nitric oxide scavenger and nitric oxide synthase inhibitor. *Jpn J Cancer Res* 1994; **85**: 331–34.

18 Maeda H, Wu J, Okamoto T, Maruo K, Akaike T. Kallikrein-kinin in infection and cancer. *Immunopharmacology* 1999; **43**: 115–28.

19 Wu J, Akaike T, Maeda H. Modulation of enhanced vascular permeability in tumors by a bradykinin antagonist, a cyclooxygenase inhibitor, and a nitric oxide scavenger. *Cancer Res* 1998; **58**: 159–65.

20 Wu J, Akaike T, Hayashida K, Okamoto T, Okuyama A, Maeda H. Enhanced vascular permeability in solid tumor involving peroxynitrite and matrix metalloproteinase. *Jpn J Cancer Res* 2001; **92**: 439–51.

21 Maeda H. The enhanced permeability and retention (EPR) effect in tumor vasculature: the key role of tumor-selective macromolecular drug targeting. *Adv Enzyme Regul* 2001; **41**: 189–207.

22 Maeda H, Sawa T, Konno T. Mechanism of tumor-targeted delivery of macromolecular drugs, including the EPR effect in solid tumor and clinical overview of the prototype polymeric drug SMANCS. *J Cont Release* 2001; **74**: 47–61.

23 Kaminishi H, Cho T, Itoh T *et al.* Vascular permeability enhancing activity of *Porphyromonas gingivalis* protease in guinea pigs. *FEMS Microbiol Lett* 1993; **114**: 109–14.

24 Kaminishi H, Hamatake H, Cho T *et al.* Activation of blood clotting factors by microbial proteinases. *FEMS Microbiol Lett* 1994; **121**: 327–32.

25 Kaminishi H, Miyaguchi H, Tamaki T *et al.* Degradation of humoral host defense by *Candida albicans* proteinase. *Infect Immun* 1995; **63**: 984–88.

26 Matsumoto K, Yamamoto T, Kamata R, Maeda H. Pathogenesis of serratial infection: activation of the Hageman factor-prekallikrein cascade by serratial protease. *J Biochem* 1984; **96**: 739–49.

27 Kamata R, Yamamoto T, Matsumoto K, Maeda H. A serratial protease causes vascular permeability reaction by activation of the Hageman factor-dependent pathway in guinea pigs. *Infect Immun* 1985; **48**: 747–53.

28 Molla A, Yamamoto T, Akaike T, Miyoshi S, Maeda H. Activation of Hageman factor and prekallikrein and generation of kinin by various microbial proteinases. *J Biol Chem* 1989; **264**: 10589–94.

29 Maeda H. Role of microbial proteases in pathogenesis. *Microbiol Immunol* 1996; **40**: 685–99.

30 Maeda H. Microbial proteinases and pathogenesis of infection. In: Creighton TE, ed. *Wiley Encyclopedia of Molecular Medicine*. New York: John Wiley & Sons, 2002; **4**: 2663–68.

31 Maruo K, Akaike T, Inada Y, Ohkubo I, Ono T, Maeda H. Effect of microbial and mite proteases on low and high molecular weight kininogens. *J Biol Chem* 1993; **268**: 17711–15.

32 Matsumura Y, Kimura M, Yamamoto T, Maeda H. Involvement of the kinin-generating cascade in enhanced vascular permeability in tumor tissue. *Jpn J Cancer Res* 1988; **79**: 1327–34.

33 Matsumura Y, Maruo K, Kimura M, Yamamoto T, Konno T, Maeda H. Kinin-generating cascade in advanced cancer patients and in vitro study. *Jpn J Cancer Res* 1991; **82**: 732–41.

34 Matsumura Y, Kimura M, Kato H, Yamamoto T, Maeda H. Quantification, isolation and structural determination of bradykinin and hydroxyprolyl-bradykinin in tumor ascites. *Adv Exp Med Biol* 1989; **247A**: 587–92.

35 Bhoola K, Ramsaroop R, Plendl J, Cassim B, Dlamini Z, Naicker S. Kallikrein and kinin receptor expression in inflammation and cancer. *Biol Chem* 2001; **382**: 77–89.

36 Wu J, Akaike T, Hayashida K *et al.* Identification of bradykinin receptors in clinical cancer specimens and murine tumor tissues. *Int J Cancer* 2002; **98**: 29–35.

37 Whalley ET, Figueroa CD, Gera L, Bhoola KD. Discovery and therapeutic potential of kinin receptor antagonists. *Expert Opin Drug Discov* 2012; **7**: 1129–48.

38 Figueroa CD, Ehrenfeld P, Bhoola KD. Kinin receptors as targets for cancer therapy. *Expert Opin Ther Targets* 2012; **16**: 299–312.

39 Oda T, Akaike T, Hamamoto T, Suzuki F, Hirano T, Maeda H. Oxygen radicals in influenza-induced pathogenesis and treatment with pyran polymer-conjugated SOD. *Science* 1989; **244**: 974–76.

40 Akaike T, Ando M, Oda T *et al.* Dependence on O_2^- generation by xanthine oxidase of pathogenesis of influenza virus infection in mice. *J Clin Invest* 1990; **85**: 739–45.

41 Maeda H, Akaike T. Oxygen free radicals as pathogenic molecules in viral diseases. *Proc Soc Exp Biol Med* 1991; **198**: 721–27.

42 Maeda H. Paradigm shift in microbial pathogenesis: an alternative to the Koch-Pasteur paradigm on the new millennium. In: ed. Arai S, Kurume University School of Medicine. Abstr. in the Proceedings of the 13th International Congress for Mycoplasmology; 14–19 July 2000, Fukuoka, Japan.

43 Akaike T, Noguchi Y, Ijiri S *et al.* Pathogenesis of influenza virus-induced pneumonia: involvement of both nitric oxide and oxygen radicals. *Proc Natl Acad Sci USA* 1996; **93**: 2448–53.

44 Yoshitake J, Akaike T, Akuta T *et al.* Nitric oxide as an endogenous mutagen for Sendai virus without antiviral activity. *J Virol* 2004; **78**: 8709–19.

45 Akaike T, Maeda H. Nitric oxide and virus infection. *Immunology* 2000; **101**: 300–8.

46 Akaike T, Maeda H. Pathophysiological effects of high-output production of nitric oxide. In: Ignarro LJ, ed. *Nitric Oxide.* San Diego: Academic Press, 2000; 733–45.

47 Akaike T, Okamoto S, Sawa T *et al.* 8-Nitroguanosine formation in viral pneumonia and its implication for pathogenesis. *Proc Natl Acad Sci USA* 2003; **100**: 685–90.

48 Akaike T, Fujii S, Kato A *et al.* Viral mutation accelerated by nitric oxide production during infection in vivo. *FASEB J* 2000; **14**: 1447–54.

49 Kuwahara H, Kariu T, Fan J, Maeda H. Generation of drug-resistant mutants of *Helicobacter pylori* in the presence of peroxynitrite, a derivative of nitric oxide, at pathophysiological concentration. *Microbiol Immunol* 2009; **52**: 1–7.

50 Kuwahara H, Kanazawa A, Wakamatsu D *et al.* Antioxidative and antimutagenic activities of 4-vinyl-2,6-dimethoxyphenol (canolol) isolated from canola oil. *J Agric Food Chem* 2004; **52**: 4380–87.

51 Cao X, Tsukamoto T, Seki T *et al.* 4-Vinyl-2,6-dimethoxyphenol (canolol) suppresses oxidative stress and gastric carcinogenesis in *Helicobacter pylori*-infected carcinogen-treated Mongolian gerbils. *Int J Cancer* 2008; **122**: 1445–54.

52 Maeda H, Akaike T. Nitric oxide and oxygen radicals in infection, inflammation, and cancer. *Biochemistry (Moscow)* 1998; **63**: 1007–17.

53 Sawa T, Akaike T, Ichimori K *et al.* Superoxide generation mediated by 8-nitroguanosine, a highly redox-active nucleic acid derivative. *Biochem Biophys Res Commun* 2003; **311**: 300–6.

54 Sato K, Akaike T, Kojima Y, Ando M, Nagao M, Maeda H. Evidence of direct generation of oxygen free radicals from heterocyclic amines by NADPH/cytochrome P-450 reductase in vitro. *Jpn J Cancer Res* 1992; **83**: 1204–9.

55 Sato K, Akaike T, Suga M, Ando M, Maeda H. Generation of free radicals from neocarzinostatin mediated by NADPH/cytochrome P-450 reductase via activation of enediyne chromophore. *Biochem Biophys Res Commun* 1994; **205**: 1716–23.

56 Kanazawa A, Sawa T, Akaike T, Maeda H. Dietary lipid peroxidation products and DNA damage in colon carcinogenesis. *Eur J Lipid Sci Technol* 2002; **104**: 439–47.

57 Maeda H, Sato K, Akaike T. Superoxide radical generation from heterocyclic amines. In: Adamson RH, Gustafsson JA, Ito N *et al.* eds. *Heterocyclic Amines in Cooked Foods: Possible Human Carcinogens.* Proceedings of the 23rd International Symposium of the Princess Takamatsu Cancer Research Fund, Tokyo. Princeton, NJ: Princeton Scientific Publishing Co., 1995; 103–12.

58 Niles JC, Wishnok JS, Tannenbaum SR. Peroxynitrite-induced oxidation and nitration products of guanine and 8-oxoguanine: structures and mechanisms of product formation. *Nitric Oxide* 2006; **14**: 109–21.

59 Sawa T, Ohshima H. Nitrative DNA damage in inflammation and its possible role in carcinogenesis. *Nitric Oxide* 2006; **14**: 91–100.

60 Okada F, Nakai K, Kobayashi T *et al.* Inflammatory cell-mediated tumour progression and minisatellite mutation correlate with the decrease of antioxidative enzymes in murine fibrosarcoma cells. *Br J Cancer* 1999; **79**: 377–85.

61 Okada F, Kobayashi M, Tanaka H *et al.* The role of nicotinamide adenine dinucleotide phosphate oxidase-derived reactive oxygen species in the acquisition of metastatic ability of tumor cells. *Am J Pathol* 2006; **169**: 294–302.

62 Okada F, Tazawa H, Kobayashi T, Kobayashi M, Hosokawa M. Involvement of reactive nitrogen oxides for acquisition of metastatic properties of benign tumors in a model of inflammation-based tumor progression. *Nitric Oxide* 2006; **14**: 122–9.

63 Okada F. Beyond foreign-body-induced carcinogenesis: impact of reactive oxygen species derived from inflammatory cells in tumorigenic conversion and tumor progression. *Int J Cancer* 2007; **121**: 2364–72.

64 Shimizu T, Marusawa H, Endo Y, Chiba T. Inflammation-mediated genomic instability: roles of activation-induced cytidine deaminase in carcinogenesis. *Cancer Sci* 2012; **103**: 1201–6.

65 Muto Y, Moriwaki H, Ninomiya M *et al.* Prevention of second primary tumors by an acyclic retinoid, polyprenoic acid, in patients with hepatocellular carcinoma. Hepatoma Prevention Study Group. *N Engl J Med* 1996; **334**: 1561–67.

66 Tanaka T, Maeda M, Kohno H *et al.* Inhibition of azoxymethane-induced colon carcinogenesis in male F344 rats by the citrus limonoids obacunone and limonin. *Carcinogenesis* 2001; **22**: 193–98.

67 Surh YJ. Cancer chemoprevention with dietary phytochemicals. *Nat Rev Cancer* 2003; **3**: 768–80.

68 Weinberg RA. *The Biology of Cancer.* New York: Garland Science, Taylor and Francis Group, 2007.

69 Maeda H. SMANCS and polymer-conjugated macromolecular drugs: advantages in cancer chemotherapy. *Adv Drug Deliv Rev* 2001; **46**: 169–85.

70 Li CJ, Miyamoto Y, Kojima Y, Maeda H. Augmentation of tumor delivery of macromolecular drugs with reduced bone marrow delivery by elevating blood pressure. *Br J Cancer* 1993; **67**: 975–80.

71 Kimura N, Taniguchi S, Aoki K, Baba T. Selective localization and growth of *Bifidobacterium bifidum* in mouse tumors following intravenous administration. *Cancer Res* 1980; **40**: 2060–68.

72 Skinner SA, Tutton PJM, O'Brien PE. Microvascular architecture of experimental colon tumors in the rat. *Cancer Res* 1990; **50**: 2411–17.

73 Daruwalla J, Nikfarjam M, Greish K *et al.* In vitro and in vivo evaluation of tumor targeting SMA-pirarubicin micelles: survival improvement and inhibition of liver metastases. *Cancer Sci* 2010; **101**: 1866–74.

74 Daruwalla J, Greish K, Wilson C *et al.* Styrene maleic acid-pirarubicin disrupts tumor microcirculation and enhances the permeability of colorectal liver metastases. *J Vasc Res* 2009; **46**: 218–28.

75 Iwai K, Maeda H, Konno T. Use of oily contrast medium for selective drug targeting to tumor: enhanced therapeutic effect and X-ray image. *Cancer Res* 1984; **44**: 2115–21.

76 Maeda H. Tumor-selective delivery of macromolecular drugs via the EPR effect: background and future prospects. *Bioconjug Chem* 2010; **21**: 797–802.

77 Maeda H. Vascular permeability in cancer and infection as related to macromolecular drug delivery, with emphasis on the EPR effect for tumor-selective drug targeting. *Proc Jpn Acad Ser B* 2012; **88**: 53–71.

78 Fang J, Nakamura H, Maeda H. EPR effect: the unique characteristics of tumor blood vessels for drug delivery, factors involved, its limitation and augmentation. *Adv Drug Deliv Rev* 2011; **63**: 136–151.

79 Maeda H, Nakamura H, Fang J. The EPR effect for macromolecular drug delivery to solid tumors: improvement of tumor uptake, lowering of systemic toxicity, and distinct tumor imaging in vivo. *Adv Drug Deliv Rev* 2013; **65**: 71–79.

80 Winchell HS, Sanchez PD, Watanabe CK, Hollander L, Anger HO, McRae J. Visualization of tumors in humans using [67] Ga-citrate and the Anger whole-body scanner, scintillation camera and tomographic scanner. *J Nucl Med* 1970; **11**: 459–60.

81 Iwai K, Maeda H, Konno T *et al.* Tumor targeting by arterial administration of lipids: rabbit model with VX2 carcinoma in the liver. *Anticancer Res* 1987; **7**: 321–8.

82 Konno T, Maeda H, Yokoyama I *et al.* Use of a lipid lymphographic agent, lipiodol, as a carrier of high molecular weight antitumor agent, SMANCS, for hepatocellular carcinoma. *Cancer Chemother* 1982; **9**: 2005–15 (in Japanese).

83 Konno T, Maeda H, Iwai K *et al.* Effect of arterial administration of high-molecular-weight anticancer agent SMANCS with lipid lymphographic agent on hepatoma: a preliminary report. *Eur J Cancer Clin Oncol* 1983; **19**: 1053–65.

84 Konno T, Maeda H, Iwai K *et al.* Selective targeting of anti-cancer drug and simultaneous image enhancement in solid tumors by arterially administered lipid contrast medium. *Cancer* 1984; **54**: 2367–74.

85 Maki S, Konno T, Maeda H. Image enhancement in computerized tomography for sensitive diagnosis of liver cancer and semiquantitation of tumor selective drug targeting with oily contrast medium. *Cancer* 1985; **56**: 751–57.

86 Konno T, Maeda H. Targeting chemotherapy of hepatocellular carcinoma. In: Okuda K, Ishak KG, eds. *Neoplasms of the Liver.* Tokyo, Berlin, Heidelberg, New York: Springer-Verlag, 1987; 343–52.

87 Kobayashi M, Imai K, Sugihara S, Maeda H, Konno T, Yamanaka H. Tumor-targeted chemotherapy with lipid contrast medium and macromolecular anticancer drug (SMANCS) for renal cell carcinoma. *Urology* 1991; **37**: 288–94.

88 Tsuchiya K, Uchida T, Kobayashi M. Long-term survival rate after tumor-targeted chemotherapy with the macromolecular anticancer drug SMANCS in lipid contrast medium for renal cell carcinoma: preoperative therapy for nonmetastatic cases. *Urology* 2000; **55**: 495–500.

89 Nagamitsu A, Greish K, Maeda H. Elevating blood pressure as a strategy to increase tumor targeted delivery of macromolecular drug SMANCS: cases of advanced solid tumors. *Jpn J Clin Oncol* 2009; **39**: 756–66.

90 Maeda H. Macromolecular therapeutics in cancer treatment: the EPR effect and beyond. *J Control Release* 2012; **164**: 138–44.

91 Konerding MA, Miodonski AJ, Lametschwandtner A. Microvascular corrosion casting in the study of tumor vascularity: a review. *Scanning Microsc* 1995; **9**: 1233–44.

92 Hashizume H, Baluk P, Morikawa S *et al.* Openings between defective endothelial cells explain tumor vessel leakiness. *Am J Pathol* 2000; **1561**: 1363–80.

93 Maeda H, Fang J, Inuzuka T, Kitamoto Y. Vascular permeability enhancement in solid tumor: various factors, mechanisms involved and its implications. *Int Immunopharmacol* 2003; **3**: 319–28.

94 Maeda H, Akaike T, Wu J, Noguchi Y, Sakata Y. Bradykinin and nitric oxide in infectious disease and cancer. *Immunopharmacology* 1996; **33**: 222–30.

95 Tanaka S, Akaike T, Wu J *et al.* Modulation of tumor-selective vascular blood flow and extravasation by the stable prostaglandin I_2 analogue beraprost sodium. *J Drug Target* 2003; **11**: 45–52.

96 Seki T, Fang J, Maeda H. Enhanced delivery of macromolecular antitumor drugs to tumors by nitroglycerin application. *Cancer Sci* 2009; **100**: 2426–30.

97 Fang J, Qin H, Nakamura H, Tsukigawa K, Shin T, Maeda H. Carbon monoxide, generated by heme oxygenase-1, mediates the enhanced permeability and retention (EPR) effect of solid tumor. *Cancer Sci* 2012; **102**: 535–41.

98 Yasuda H, Yamaya M, Nakayama K *et al.* Randomized phase II trial comparing nitroglycerin plus vinorelbine and cisplatin with vinorelbine and cisplatin alone in previously untreated stage IIIB/IV non-small cell lung cancer. *J Clin Oncol* 2006; **24**: 688–94.

99 Yasuda H, Nakayama K, Watanabe M *et al.* Nitroglycerin treatment may increase response to docetaxel and carboplatin regimen via inhibitions of hypoxia-inducible factor-1 pathway and P-glycoprotein in patients with lung adenocarcinoma. *Clin Cancer Res* 2006; **12**: 6748–57.

100 Yasuda H, Yanagihara K, Nakayama K *et al.* Therapeutic applications of nitric oxide for malignant tumor in animal models and human studies. In: Bonavida B, ed. *Nitric Oxide and Cancer.* New York: Springer Science, 2010; 419–441.

101 Jordan BF, Misson P, Demeure R, Baudelet C, Beghein N, Gallez B. Changes in tumor oxygenation/perfusion induced by the NO donor, isosorbide dinitrate, in comparison with carbogen: monitoring by EPR and MRI. *Int J Radiat Oncol Biol Phys* 2000; **48**: 565–70.

102 Mitchell JB, Wink DA, DeGraff W, Gamson J, Keefer LK, Krishna MC. Hypoxic mammalian cell radiosensitization by nitric oxide. *Cancer Res* 1993; **53**: 5845–8.

103 Noguchi A, Takahashi T, Yamaguchi T *et al.* T. Enhanced tumor localization of monoclonal antibody by treatment with kininase II inhibitor and angiotensin II. *Jpn J Cancer Res* 1992; **83**: 240–3.

104 Nakamura H, Liao L, Hitaka Y *et al.* Micelles of zinc protoporphyrin conjugated to *N*-(2-hydroxypropyl)methacrylamide (HPMA) copolymer for imaging and light-induced antitumor effects in vivo. *J Control Release* 2013; **165**: 191–8.

105 Iyer A, Greish K, Seki T *et al.* Polymeric micelles of zinc protoporphyrin for tumor targeted delivery based on EPR effect and singlet oxygen generation. *J Drug Target* 2007; **15**: 496–506.

106 Funkhouser J. Reinventing pharma: the theranostic revolution. *Curr Drug Discov* 2002; **2**: 17–9.

107 Kelkar S, Reineke T. Theranostics: combining imaging and therapy. *Bioconjug Chem* 2011; **22**: 1879–1903.

108 Hatakeyama H, Akita H, Kogure K, Harashima H. Development of a novel systemic gene delivery system for cancer therapy with a tumor-specific cleavable PEG-lipid. *Gene Ther* 2007; **14**: 68–77.

109 Nakamura H, Fang J, Gahininath B, Tsukigawa K, Maeda H. Intracellular uptake and behavior of two types zinc protoporphyrin (ZnPP) micelles, SMA-ZnPP and PEG-ZnPP as anticancer agents; unique intracellular disintegration of SMA micelles. *J Control Release* 2011; **155**: 367–75.

110 Oda T, Maeda H. Binding to and internalization by cultured cells of neocarzinostatin and enhancement of its actions by conjugation with lipophilic styrene-maleic acid copolymer. *Cancer Res* 1987; **47**: 3206–11.

111 Oda T, Sato F, Maeda H. Facilitated internalization of neocarzinostatin and its lipophilic polymer conjugate, SMANCS, into cytosol in acidic pH. *J Nat Cancer Inst* 1987; **9**: 1205–11.

112 Oda T, Morinaga T, Maeda H. Stimulation of macrophage by polyanions and its conjugated proteins and effect on cell membrane. *Proc Soc Exp Biol Med* 1986; **181**: 9–17.

113 Duncan R, Gaspar R. Nanomedicine(s) under the microscope. *Mol Pharm* 2011; **8**: 2101–41.

114 Kano M, Bae C, Iwata Y *et al.* Improvement of cancer-targeting therapy, using nanocarriers for intractable solid tumors by inhibition of TGF-β signaling. *Proc Natl Acad Sci U S A* 2007; **104**: 3460–65.

115 Seki T, Carroll F, Illingworth S *et al.* Tumour necrosis factor-alpha increases extravasation of virus particles into tumour tissue by activating the Rho A/Rho kinase pathway. *J Control Release* 2011; **156**: 381–89.

116 Gormley AJ, Larson N, Sadekar S, Robinson R, Ray A, Ghandehari H. Guided delivery of polymer therapeutics using plasmonic photothermal therapy. *Nano Today* 2012; **7**: 158–67.

Protection from inflammatory bowel disease and colitis-associated carcinogenesis with 4-vinyl-2,6-dimethoxyphenol (canolol) involves suppression of oxidative stress and inflammatory cytokines

Jun Fang[1–3,†], Takahiro Seki[2,4,8,†], Tetsuya Tsukamoto[5],
Haibo Qin[1,6], Hongzhuan Yin[1,7], Long Liao[1,6],
Hideaki Nakamura[1,2] and Hiroshi Maeda[1,2,*]

[1]Research Institute for Drug Delivery System and [2]Laboratory of
Microbiology and Oncology, Faculty of Pharmaceutical Sciences, Sojo
University, Kumamoto 860-0082, Japan, [3]Department of Toxicology, Anhui
Medical University, Hefei 230032, P. R. China, [4]Regional Cooperative
Research Center, Kumamoto University, Kumamoto 861-2202, Japan,
[5]Department of Diagnostic Pathology, Fujita Health University School
of Medicine, Toyoake, Aichi 470-1192, Japan, [6]Department of Applied
Microbiology, Sojo University, Kumamoto 860-0082, Japan and [7]Department
of General Surgery, Sheng Jing Hospital, China Medical University,
Shenyang 110004, P. R. China

[8]Present address: Laboratory of Angiogenesis Research, Department of
Microbiology, Tumor and Cell Biology, Karolinska Institute, Nobels väg 16,
SE-171 77, Stockholm, Sweden

*To whom correspondence should be addressed. Tel: +81-96-326-4114;
Fax: +81-96-326-3158;
Email: hirmaeda@ph.sojo-u.ac.jp

Oxidative stress is associated with various pathological processes including inflammatory bowel disease, which is a major cause of colon cancer. Here, we examined the antioxidative and anti-inflammatory effects of 4-vinyl-2,6-dimethoxyphenol (canolol), a potent antioxidant compound obtained from crude canola oil. Oral administration of 2% dextran sulfate sodium (DSS) resulted in the progression of colitis with shortening of the large bowel length. Administering a diet containing canolol significantly suppressed pathogenesis; diarrhea markedly improved and the length of large bowel returned to almost normal. Pathological examination clearly revealed improvement of colonic ulcers. Production of inflammatory cytokines, i.e. interleukin-12 and tumor necrosis factor-α, was significantly increased during this pathological process; their production was markedly inhibited by canolol. In the azoxymethane/DSS-induced colon cancer model, mice receiving canolol had a reduced occurrence of cancer, to 60%, compared with control mice, 100% of which had colon cancer. The numbers of tumors in each mouse were also significantly reduced in mice receiving the canolol-containing diet (5.6±2.0) compared with azoxymethane/DSS control mice (10.8±4.2). No apparent toxicity of canolol was observed. Moreover, inflammatory cytokines (i.e. cyclooxygenase-2, inducible nitric oxide synthase and tumor necrosis factor-α) and oxidative responding molecules, i.e. heme oxygenase-1, in colon were suppressed during this treatment. In a mouse colon 26 solid tumor model, canolol significantly suppressed cyclooxygenase-2 expression; however, no significant tumor growth inhibition was observed, suggesting that canolol preferably shows chemopreventive effects during the stages of initiation/promotion. Canolol may, thus, be considered a potential cancer preventive agent or supplement.

Abbreviations: 8-OHdG, 8-hydroxydeoxyguanosine; AOM, azoxymethane; BHT, butylated hydroxytoluene; COX-2, cyclooxygenase-2; DAI, disease activity index; DSS, dextran sulfate sodium; ELISA, enzyme-linked immunosorbent assay; HO-1, heme oxygenase-1; IBD, inflammatory bowel disease; IL-12, interleukin-12; iNOS, inducible NO synthase; LPS, lipopolysaccharide; NO, nitric oxide; ROS, reactive oxygen species; SIN-1, 3-(4-morpholinyl)sydnonimine hydrochloride; TNF-α, tumor necrosis factor-α.

†These authors contributed equally to this work.

Introduction

Inflammatory bowel disease (IBD) comprises a group of common diseases that manifest chronic inflammation of the colon and small intestine (1–3). The major types of IBD are Crohn's disease and ulcerative colitis. Although IBD itself is rarely fatal, it can greatly diminish the quality of life because of pain, vomiting, diarrhea and other socially unacceptable symptoms. More important, patients with IBD commonly have an increased risk of colorectal cancer, i.e. the risk of colon cancer in patients with ulcerative colitis begins to rise significantly above that of the general population approximately 8–10 years after diagnosis (1–4).

At present, a common therapeutic modality for IBD is use of anti-inflammatory agents, including sulfasalazine (Salazopyrin) and acetylsalicylic acid, steroid hormone and other immunosuppressive agents. Most of these treatments are symptomatic and palliative because the etiology of the disease is not yet established. As a result, the disease persists for a long time. Therefore, a therapeutic/preventive strategy that is based on the mechanism of IBD is an urgent necessity.

Although the exact cause of IBD must be determined, dysfunctional immunoregulation is thought to be the primary reason (1–4). Genetic, infectious, immunological, and psychological factors have also been implicated as influencing the development of IBD. Recently it was also reported that, similar to *Helicobacter pylori*-induced gastritis, bacterial infection may be involved in pathogenesis of IBD, and combination therapy with antibiotics produced a significant therapeutic effect (5–8).

Another possibility concerns reactive oxygen species (ROS): high levels were produced in IBD, which suggests that ROS may be implicated in the molecular etiology of IBD (9,10). The destructive effects of ROS on DNA, proteins and lipids, because of the highly reactive nature of ROS, may contribute to initiation and propagation of the disease (6,7). The investigation of antioxidant agents may, thus, help illuminate the etiology, treatment and prevention of IBD. Indeed, many researchers proved antioxidant treatment of IBD to be effective, not only in animal experiments but also in clinical settings (9,11).

In our laboratory, we identified a potent antioxidant phenolic compound in crude canola (rapeseed) oil, 4-vinyl-2,6-dimethoxyphenol (canolol), which exhibits a more potent alkylperoxyl (ROO˙) radical scavenging activity than many well-known antioxidants, such as α-tocopherol, vitamin C, β-carotene, rutin and quercetin (12). Recently canolol was also found in mustard seed oil (13). We previously reported a strong inhibitory capacity of canolol against the endogenous mutagen peroxynitrite (ONOO⁻), which is a potent oxidizing and nitrating agent, and suppression by canolol of bacterial mutation, via protection from DNA damage (14,15). In related studies, we demonstrated a protective effect of canolol against gastritis and gastric ulcers and a preventive effect on gastric carcinogenesis in the *H.pylori*-infected, carcinogen-treated Mongolian gerbil, which is an excellent animal model of *H.pylori*-induced, chronic active gastritis similar to IBD and involving ROS (16).

Addition of dextran sulfate sodium (DSS) to the drinking water of mice induced acute colitis characterized by bloody diarrhea, ulceration and inflammatory infiltration of leukocytes in the colon, as a result of toxicity to gut epithelial cells and distortion of the integrity of the mucosal barrier (17). The DSS-induced colitis model, which we used in this study, is commonly utilized as a model of inflammatory colitis (5,6). Application of azoxymethane (AOM) together with DSS produces a model of chronic colitis and colitis-associated colon carcinogenesis (18). The purpose of our present study was to evaluate the effectiveness of canolol for inhibition of IBD and

colitis-associated carcinogenesis using a DSS-induced mouse colitis model and AOM/DSS-induced colon carcinogenesis in mice, respectively. We also investigated the effect of canolol on oxidative stress and inflammatory cytokines during development of colitis and colon carcinogenesis. The toxicity of canolol and its effect on a mouse colon 26 solid tumor model were also examined.

Material and Methods

Chemicals

Canolol (molecular weight, 180 Da), with >95% purity, was synthesized by Junsei Chemical Co., Ltd. (Tokyo, Japan). Antioxidant 2,6-di-*tert*-butyl-4-methylphenol [butylated hydroxytoluene (BHT), Sigma, St Louis, MO] was added to canolol solution (in ethanol) at the concentration of 300 ppm. BHT at this concentration had no significant therapeutic effect on colitis and colon cancer prevention (16). The preparation in solid form or solution was sealed under helium or nitrogen, and stock solution in ethanol was kept at −80°C. DSS was purchased from Wako Pure Chemical (Osaka, Japan), and AOM was from Sigma. 3-(4,5-Dimethyl-2-thiazolyl)-2,5-diphenyl-2H-tetrazolium bromide was purchased from Dojindo Chemical Laboratory (Kumamoto, Japan).

Diets

The AIN93G diet containing canolol was used in this study with some modifications. Components of the modified AIN93G diet are as follows (g/kg): corn starch, 397; casein, 200; α-corn starch, 132; sucrose, 100; soybean oil, 70; cellulose, 50; AIN93G mineral mixture, 35; AIN93G vitamin mixture, 10; L-cystine, 3.0; choline bitartrate, 2.5; and BHT, 0.014. L-Cystine and BHT were purchased from Sigma; other components were from Oriental Yeast Co., Ltd (Tokyo, Japan). Canolol was first dissolved in soybean oil and then mixed into the diet to the concentration of 0.1 or 0.3%. The control diet contained the same components but no canolol. The diets were sealed under vacuum and were stored at −30°C; they were given daily after being thawed. Each day, leftovers from the previous day's feeding were measured, and new food was provided to replace the amount eaten.

Cell culture

Human embryonic kidney cells HEK293 and human colon cancer cells Caco-2 were cultured in Dulbecco's modified Eagle's medium (Invitrogen, Carlsbad, CA), and mouse colon cancer cells colon 26 were cultured in Roswell Park Memorial Institute 1640 medium (Invitrogen), at 37°C in an atmosphere of 5% CO_2/95% air.

Animals and experimental protocol

Female ICR mice, 6 weeks old and weighing 20 to 25 g, and female BALB/c mice, 8 weeks old, were obtained from Kyudo (Tosu city, Saga, Japan). All animals were maintained under standard conditions and were fed water and murine chow *ad libitum*. All experiments were carried out according to the Guidelines of the Laboratory Protocol of Animal Handling, Sojo University, and were approved by the Animal Care Committee of Sojo University.

As to the experimental protocol for the DSS-induced colitis model, ICR mice of canolol treatment groups were fed with diet containing different concentrations of canolol during the entire experimental period (7 days). Control ICR mice were fed with the same diets but without canolol. Two hours after feeding canolol-containing diet, water containing 2% DSS was supplied to all groups except the healthy normal ICR mouse group, for entire 7 days (Supplementary Figure 1A, available at *Carcinogenesis* Online). Fresh diet was supplied daily, and the body weights of mice and amounts of consumed diet were determined each day. According to this protocol, symptoms indicating the severity of colitis obtained by macroscopic observation, such as characteristics of fecal pellets, diarrhea and hematochezia, were recorded. On day 7, the mice were killed, and specimens of blood, colon and liver were collected for biochemical and pathological examinations. After the length of each colon was measured, the colon specimen was fixed with 20% formalin solution and embedded in paraffin. Paraffin-embedded sections (6 μm thick) were prepared as usual for histological examination after hematoxylin and eosin staining, as well as for immunohistochemical staining as described below. Serum obtained from the blood collected was used to determine levels of tumor necrosis factor-α (TNF-α) and interleukin-12 (IL-12), as described below.

As to the experimental protocol for colon carcinogenesis in ICR mice induced by AOM/DSS, on day 1, AOM (at 10 mg/kg) dissolved in saline was administered intraperitoneally, and after 1 week, 2% DSS was given orally in the drinking water for 1 week. The diet was changed to the canolol-containing diet from 2 h before AOM administration and was continued for the

entire experimental period of 6 weeks (Supplementary Figure 1B, available at *Carcinogenesis* Online). The amount of food consumed was calculated daily. Six weeks after the AOM injection, mice were killed, and colon and liver specimens were collected. The numbers of tumors in the colon of each mouse were measured.

Evaluation of colitis severity

We evaluated the colitis severity by measuring disease activity index (DAI) semiquantitatively, by measuring colon length as an indirect marker of inflammation, and by using histology after hematoxylin and eosin staining. The DAI was determined by scoring changes in animal weight, presence of occult blood, gross bleeding and stool consistency, as described in the literature (19). We used five grades of weight loss (0: either a gain of weight or no weight loss; 1: 1% to 5% loss; 2: 5% to 10% loss; 3: 10% to 20% loss; 4: more than 20% loss), three grades of stool consistency (0: normal; 2: loose; and 4: diarrhea) and three grades of occult blood (0: negative; 2: occult blood-positive; and 4: gross bleeding). Individual mice were graded, and the mean value for each experimental group was obtained.

Further, histological evaluation of ulcer was carried out to quantitate the degree of colitis. The numbers of ulcer regions were counted in whole-colon mucosa and divided by the total length of the evaluated colon specimens. The numbers of ulcers are expressed in unit length (mm).

Effect of canolol on colon 26 transplanted tumor

The effect of canolol on tumor was further investigated in a mouse colon cancer model. Cultured colon 26 cells (2×10^6) were implanted subcutaneously in the dorsal skin of Balb/c mice. Ten days after tumor inoculation, when tumor reached a diameter of 5–6 mm, canolol (dissolved in corn oil) was orally administration at the dose of 100 mg/kg (0.1 ml), and corn oil without canolol was used for control mice. Administration was carried out every second day, totally for three times. Growth of the tumors was monitored every 2–3 days by measuring tumor volume with a digital caliper, which was estimated by measuring longitudinal cross-section (*L*) and transverse section (*W*) according to the formula $V = (L \times W^2)/2$. On day 15 after the first canolol administration when tumor reached a diameter ~12–13 mm, mice were killed and tumor tissues were excised for histological examination and immunohistochemical analysis as described below.

Immunohistochemical analyses of cyclooxygenase-2

Expressions of cyclooxygenase-2 (COX-2) in colon mucosa of mice with DSS-induced colitis and in mice with AOM/DSS-induced colon carcinogenesis, and also in colon 26-implanted syngeneic solid tumor, were detected immunohistochemically as described previously (16), using a rabbit anti-mouse COX-2 polyclonal antibody (diluted 1:500, Cayman Chemical, Ann Arbor, MI) with 3,3′-diaminobenzidine (Wako Pure Chemical) for visualization. Images were analyzed with ImageJ software (National Institutes of Health, Bethesda, MD) for brown deposition of 3,3′-diaminobenzidine as COX-2 positive. One pathologist (T.T.) who was not informed about the samples examined the immunostained slides.

To quantitate the degree of staining, numbers of COX-2-positive cells were counted in whole-colon mucosa in DSS-induced colitis experiment, or counted in a distal quarter of colon mucosa, which is the target region of AOM/DSS in colon carcinogenesis experiment, and divided by the total length of the evaluated colon specimens to compare each sample equally. The numbers of COX-2-positive cells are illustrated in unit length (mm).

In the experiments using colon 26 solid tumor, three representative photographs were taken from each tumor using an AxioCam HRc digital camera and AxioVision v.4.8.2.0 software (Carl Zeiss, Oberkochen, Germany), and average positive areas in the each frame were compared between control and canolol groups.

Enzyme-linked immunosorbent assay for 8-hydroxydeoxyguanosine in the plasma of DSS-induced colitis mice with/without canolol treatment

Oxidative stress in the DSS-induced colitis mice with or without canolol treatment was examined by detecting 8-hydroxydeoxyguanosine (8-OHdG) in plasma, using an enzyme-linked immunosorbent assay (ELISA) kit (8-OHdG Check, JaICA, Fukuroi, Shizuoka, Japan). In brief, blood was drawn from the inferior vena cava after mice were killed, plasma samples were obtained by centrifugation (4°C, 5000*g* for 20 min) and DNA in each sample was then extracted using QuickGene DNA tissue kit (DT-S, Wako Pure Chemical), followed by hydrolysis using an 8-OHdG Assay Preparation Reagent Set (Wako Pure Chemical). The ELISA was then performed to detect 8-OHdG according to the manufacturer's instructions.

Effects of canolol on production of IL-12 and TNF-α in DSS-induced colitis

Serum samples from mice with DSS-induced colitis were obtained as described above, and levels of TNF-α and IL-12 were quantified by using an

ELISA kit (Pierce Biotechnology Rockford, IL) according to the manufacturer's instructions.

Inhibitory effect of canolol on activation of macrophages from the BALB/c mouse

Macrophages were obtained from the peritoneal fluid of mice stimulated with casein. In brief, 1 ml of 5% casein sodium (Wako Pure Chemical) in phosphate-buffered saline was injected intraperitoneally into BALB/c mice. After 3 days, mice were killed, and 5 ml of cold phosphate-buffered saline was injected into the peritoneal cavity, after which peritoneal lavage fluid (~5 ml) was collected, followed by centrifugation of the fluid (1000 r.p.m., 5 min) at 4°C. The macrophages were washed with phosphate-buffered saline three times by centrifugation, and then 15 ml of Roswell Park Memorial Institute 1640 medium (Invitrogen) with 10% FBS was added and macrophages were cultured in a plastic petri dish (100×26 mm; Nunc A/S, Roskilde, Denmark).

To activate the macrophages in culture, lipopolysaccharide (LPS) (1.0 µg/ml) and interferon-γ (0.1 µg/ml) (Sigma) were added to the cells for 24 h. Culture medium was then collected for measurement of the concentration of nitrite, which is formed from nitric oxide (NO). A significantly high amount of NO was generated by activated macrophages, which was attributable to the action of inducible NO synthase (iNOS). The nitrite concentration was quantified by using a Griess reagent kit (NO_2/NO_3 Assay Kit-C II; Dojindo Laboratories), according to the manufacturer's instructions. The production of inflammatory cytokines, i.e. TNF-α and IL-12, was also measured in culture media by using ELISA as mentioned above.

Protective effect of canolol against $ONOO^-$-induced cytotoxicity

HEK293 cells were plated at 3000 cells/well in a 96-well plate (Nunc A/S). After overnight preincubation, 1 mM or 2 mM 3-(4-morpholinyl)sydnonimine hydrochloride [SIN-1 (Dojindo Laboratories)], from which $ONOO^-$ was produced, was added to the cells. Canolol at various concentrations was then added. After an additional 48 h of incubation, cell viability was determined by using the 3-(4,5-dimethyl-2-thiazolyl)-2,5-diphenyl-2H-tetrazolium bromide (MTT) assay.

Expression of COX-2, TNF-α, iNOS and heme oxygenase-1 in colon tissues of AOM/DSS-induced carcinogenesis mice with/without feeding canolol

To examine the antioxidative, anti-inflammatory mechanisms of canolol in chemoprevention against AOM/DSS-induced colon carcinogenesis, mRNA expressions of representative oxidative inflammatory molecules [i.e. COX-2, TNF-α, heme oxygenase-1 (HO-1) and iNOS] were detected by reverse transcription–polymerase chain reaction. Briefly, after the protocol of AOM/DSS-induced carcinogenesis, total RNA from colon tissues of distal quarter in which most tumors were observed was extracted by using Sepasol®-RNA I Super reagent (NACALAI TESQUE, Kyoto, Japan), according to the manufacturer's instruction. The nucleotide sequences of the oligonucleotide primers and cycle conditions of PCR are as follows: COX-2: forward, 5′-ACA CAC TCT ATC ACT GGC ACC-3′; reverse, 5′-TTC AGG GAG AAG CGT TTG C-3′; 35 cycles of 15 s at 94°C, 15 s at 55°C and 1 min at 72°C to obtain a 274-bp cDNA; TNF-α: forward, 5′-CTA TGT CTC AGC CTC TTC TC-3′; reverse, 5′- CAG CCT TGT CCC TTG AAG AG -3′; 40 cycles of 15 s at 94°C, 30 s

at 56°C and 30 s at 68°C to obtain a 353-bp cDNA; HO-1: forward, 5′-GGC CCT GGA AGA GGA GAT AG-3′; reverse, 5′-GCT GGA TGT GCT TTT GGT G-3′; 30 cycles of 30 s at 94°C, 30 s at 56°C and 30 s at 72°C to obtain a 888-bp cDNA; iNOS: forward, 5′-CCC TTC CGA AGT TTC TGG CAG CAG C-3′; reverse, 5′-GGC TGT CAG AGC CTC GTG GCT TTG G-3′; 35 cycles of 1 min at 95°C, 1 min at 65°C and 2 min at 72°C to obtain a 496-bp cDNA; GAPDH (inner control): forward, 5′-CAT GTG GGC CAT GAG GTC CAC CAC-3′; reverse, 5′-TGA AGG TCG GAG TCA ACG GAT TTG GT-3′; 30 cycles of 1 min at 94°C, 1 min at 56°C and 1 min at 72°C to obtain a 983-bp cDNA. PCR products then underwent electrophoresis on ethidium bromide-stained 1.2% agarose gels.

Safety of canolol

Female ICR mice, beginning 6 weeks of age, were fed normal diet (untreated control) or 0.3% canolol for 6 weeks. Then, mice were killed, and blood samples were obtained. Red blood cell count, white blood cell count and hemoglobin levels were determined using an automated blood counter (F-800 Microcell Counter, Toa Medical Electronics, Kobe, Japan). Plasma obtained by centrifugation was used for measurement of the liver and the kidney functions including alanine aminotransferase, aspartate aminotransferase, lactate dehydrogenase, blood urea nitrogen and total creatine using a sequential multiple Auto Analyzer system (Hitachi Ltd., Tokyo, Japan).

Statistical analyses

Data were analyzed by one-way analysis of variance followed by the Bonferroni *t*-test. Some studies with two experiments were analyzed by Mann–Whitney *U*-test, and a Fisher's exact test was used to analyze the data of tumor incidence. A difference was considered statistically significant when $P < 0.05$.

Results

Protective effect of canolol against DSS-induced colitis

Severe diarrhea accompanied by hematochezia, characterized by significant increase in DAI, was observed on day 7 in the DSS-induced colitis group without canolol; these DSS-treated mice showed a decrease in body weight though no statistical significance was found (Table I). These symptoms were markedly improved with significantly decreased DAI when canolol was added to the diet in a dose-dependent manner, and these mice showed no apparent loss of body weight (Table I). Moreover, mice with DSS-induced colitis demonstrated shortening of the large bowel, which is one of the indexes of colitis, and this pathological change was significantly improved by canolol dose dependently (Table I). No significant differences in DAI and in length of large bowel were observed in mice receiving 1% of canolol compared with normal mice (Table I), suggesting an almost complete cure of colitis. However, 1% of canolol becomes impracticable as a chemopreventive agent or supplement especially for long-term application, i.e. canolol

Table I. Protective effect of canolol against DSS-induced colitis (on day 7) and AOM/DSS-induced colon carcinogenesis (at 6 weeks)

Group	Body weight (g)	Liver weight (g)	Length of large bowel (cm)	DAI[a]	
Normal	29.7±2.0	3.1±0.7	15.0±1.5**	0	
DSS	26.9±4.4	2.4±0.6	9.6±2.1	9.6±0.3	
DSS + 0.1% canolol	27.6±2.2	2.8±0.5	12.8±1.2*	5.2±0.7**	
DSS + 0.3% canolol	28.8±3.3	2.7±0.5	13.3±2.1**#	3.7±0.6**	
DSS + 1% canolol	29.3±1.5	2.9±0.1	13.7±1.7**#	1.2±1.8**#	

Group	Body weight (g)	Liver weight (g)	Length of large bowel (cm)#	Incidence and multiplicity of tumors	
				Tumor incidence (%)[b]	Tumor multiplicity (no. of tumors/animal)
Normal	48.0±4.7	2.5±0.4	13.0±0.9**	0**	0
AOM/DSS	44.0±3.3	2.0±0.2	8.7±0.6	100	10.8±4.2
AOM/DSS + 0.1% canolol	44.6±6.1	2.1±0.1	10.9±0.9*	60**	5.3±2.7*
AOM/DSS + 0.3% canolol	44.7±1.9	2.0±0.1	10.7±0.3*	57**	5.6±2.7*

Data are means ± SD, $n = 5$–14 for DSS-induced colitis experiments, and $n = 10$–20 for AOM/DSS-induced colon carcinogenesis experiments.
[a]See text for details.
[b]Statistical significance was analyzed by Fisher's exact test.
*$P < 0.05$, **$P < 0.01$, versus the DSS control group, or versus the AOM/DSS control group.
#No significant difference ($P > 0.05$), versus normal group.